Origin of Mobility Reduction in Thin a-IGZO TFTs and Its Improvement

Hanjun Cho, Masatake Tsuji, Shigenori Ueda, and Hideo Hosono

***Abstract*— The degradation of field-effect mobility with decreasing channel thickness in amorphous In-Ga-Zn-O thin-film transistors (a-IGZO TFTs) remains a critical issue with a controversial origin. Here, we propose that the mobility degradation in very thin a-IGZO TFTs originates from a defective surface layer. Simulated results reveal that the degradation is primarily governed by the broadening of unoccupied tail states below the conduction band minimum. These large tail state densities arise from enhanced structural disorder created by sputter-deposition process. As the channel thickness decreases, this defective layer becomes dominant in carrier transport. The presence of surface defect layer was revealed by hard X-ray photoelectron spectroscopy combined with ex situ wet etching. Removal of the surface defective layer by the etching led to the restoration of the mobility of the 5 nm channel thickness from 13.7 to 28.5 $cm^2/V{\cdot}s$ at 2 MV/cm, which is comparable to the thick TFTs.**

***Index Terms*— Amorphous oxide semiconductor, defect, mobility, thin-film transistor.**

I. Introduction

AMORPHOUS oxide semiconductors (AOSs), with high-field-effect mobility (μ_{FE}) (> 10 $cm^2/V{\cdot}s$), have become a de facto standard for flat-panel display backplanes [1], [2]. Recently, the development of high mobility channel materials and the reduction of channel thickness (t_{ch}) have been actively investigated for the high-density scaling in next-generation display and memory applications, including current-driven organic light-emitting diodes (OLEDs) and capacitor-free dynamic random-access memory (DRAM) [3], [4], [5]. In particular, as next-generation DRAM employs vertically stacked three-dimensional architectures to achieve higher density, t_{ch} below 10 nm are required. However, a severe degradation in μ_{FE} and instability in the ultra-thin t_{ch} below 10 nm hinder their next-generation applications [6], [7]. Proposed mechanisms for this thickness-dependent degradation primarily involve depletion effects induced by acceptor-like trap states at the back channel [8], as well as reduced doping efficiency and the formation of deep electron traps [7], [9]. Since the degradation has been attributed to surface-related traps, passivation has been commonly employed; however, recent studies show that this approach is ineffective, implying that the degradation originates from the inside film rather than the surface [6], [10]. Consistently, μ_{FE} degradation persists even in hydroxyl-free IGZO, indicating an intrinsic origin of the degradation. The quantum confinement effect has also been considered; however, it is limited to films thinner than 3 nm [11]. Recently, it was reported that intrinsic oxygen displacements formed in thinner films, which can be regarded as Frenkel defects, deepens the carrier activation energy and act as carrier traps, leading to serious TFT instability [6]. Furthermore, such intrinsic structural disorder induces local electrostatic potential fluctuations, thereby perturbing the conduction band (CB) [12]. The formation of these intrinsic defect species strongly correlates with film deposition conditions and the chemical composition. On the other hand, strategies to mitigate intrinsic defect species generated near the surface during film deposition have not been established. Moreover, in sputtered AOS films, post-annealing alone cannot effectively suppress this degradation, indicating a fundamental limitation of thermal treatment. This suggests that the dominant defects cannot be eliminated by post-annealing. Consequently, achieving high mobility in ultra-thin films where these intrinsic defects become dominant remains challenging, highlighting the need for alternative strategies such as direct removal of the defective near-surface region.

In this study, we propose a model for μ_{FE} degradation and a simple approach to overcome this thickness-dependent deterioration. We employed a bilayer model in the technology computer-aided design (TCAD) simulation, consisting of a defective surface and a clean bulk region, consistent with the defective surface layer observed by depth-resolved HAXPES. This confirms that the high density of surface tail states below the CBM is the primary cause of the μ_{FE} degradation. It is demonstrated that the removal of this defective surface layer via a wet-etching process effectively suppresses these defective states near the Fermi level (E_F), restoring the μ_{FE} of 5 nm t_{ch} TFTs to values comparable to thick-channel devices. These results indicate that the intrinsic behavior of ultra-thin AOS TFTs can be recovered when trap states originating from the near-surface region are effectively eliminated.

Received 6 May 2026; accepted 17 May 2026. Date of publication 22 May 2026; date of current version 1 July 2026. This work was supported in part by the Ministry of Education, Culture, Sports, Science and Technology (MEXT), Japan, under Grant JPMXP1122683430; in part by JSPS KAKENHI under Grant Number JP23K19266 and Grant Number JP24K17753; and in part by Samsung Electronics under Grant IO250530-13006-01. The review of this letter was arranged by Editor S. Zhang. *(Corresponding authors: Masatake Tsuji; Hideo Hosono.)*

Hanjun Cho and Masatake Tsuji are with the MDX Research Center for Element Strategy, International Research Frontiers Initiative, Institute of Science Tokyo, Yokohama 226-8501, Japan (e-mail: tsuji.m.ac@m.titech.ac.jp).

Shigenori Ueda is with the National Institute for Materials Science, Tsukuba 305-0044, Japan.

Hideo Hosono is with the MDX Research Center for Element Strategy, International Research Frontiers Initiative, Institute of Science Tokyo, Yokohama 226-8501, Japan, and also with the National Institute for Materials Science, Tsukuba 305-0044, Japan (e-mail: hosono.h.aa@m.titech.ac.jp).

Digital Object Identifier 10.1109/LED.2026.3695312

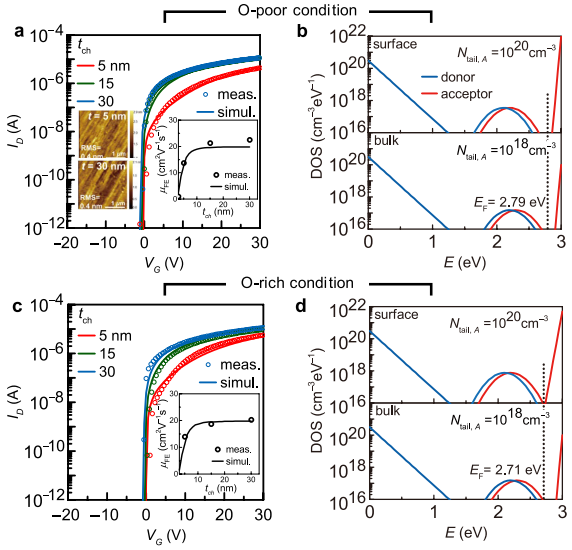

Fig. 1. Experimental and simulated transfer characteristics of (a) low P_{O2} and (c) high P_{O2}, a-IGZO TFTs with varying t_{ch}. Insets show the atomic force microscopy images of 5 and 30-nm thick films. Transfer curves were acquired at a drain–source voltage of 0.1 V. (b, d) Input DOS for the surface and bulk regions used in the simulation for the (b) low P_{O2} and (d) high P_{O2} in t_{ch} = 5 nm TFTs. The dashed lines indicate the equilibrium E_F determined by a doping carrier concentration of 1×10^{17} cm^{-3}, considering the indium-rich composition.

II. Experimental Details

Bottom-gate top-contact TFTs were fabricated on p^{++}-type Si substrates with a 150 nm-thick SiO_2 layer, using a metal shadow mask for active layer patterning to minimize impurity contamination. a-IGZO (In:Ga:Zn = 60:30:10 at.%) active layers with t_{ch} of 5–30 nm were deposited by RF sputtering using a 3-inch disk target at 150 W, a total pressure of 0.4 Pa, a base pressure of $\sim 2 \times 10^{-7}$ Pa, with $P_{O2} = O_2/Ar+O_2$ ranging from 0.25 to 25%. Etching was conducted either by a wet process using a 1.6 wt% tetramethylammonium hydroxide (TMAH) solution at 44 °C or by a dry process using Ar^+ ion sputtering. Following the etching process, the samples were annealed at 400 °C for 1 h in air. Next, Ti (5 nm)/Au (60 nm) electrodes were sputtered for the source/drain contacts. These electrodes were patterned by photolithography and a lift-off process, defining a channel width/length of 300/30 μm to avoid μ_{FE} overestimation [13], [14]. Finally, a second thermal annealing step (400 °C for 1 h in air) was performed. The degradation mechanism was analyzed by 2D TCAD simulations (Silvaco Atlas) employing a bilayer density of states (DOS) model. The DOS parameters for the a-IGZO TCAD model were extracted from literature and further calibrated using temperature-dependent AC-Hall effect measurements [7], [15], [16]. Depth-dependent electronic structures were examined using hard X-ray photoemission spectroscopy (HAXPES) in total-reflection (TR) [17], [18] and angle-resolved (AR) modes at BL09XU of SPring-8 [19]. AR-HAXPES measurements at take-off angles (TOAs) of 15° and 85° provided surface- and bulk- sensitive information with probing depths (3 times of inelastic mean-free-path of photoelectrons) of 5.7 and 19.8 nm, respectively.

III. Results and Discussion

Fig. 1a shows that for low P_{O2} a-IGZO, μ_{FE} significantly decreases from 22.5 to 13.7 cm^2/V·s as the t_{ch} decreases from 30 to 5 nm. The surface roughness remained low (root-mean-square roughness = 0.4 nm) regardless of t_{ch}, excluding morphological scattering as a dominant factor. Moreover, the degradation persists even with a passivation layer, indicating that its origin lies not in the outermost surface but in the near-surface region with a finite thickness [6]. To elucidate the intrinsic structural changes and defect-related degradation mechanism, TCAD simulations were performed. The channel layer was modeled as a bilayer consisting of a bulk region and a 2 nm-thick defective surface layer, which was experimentally eliminated by wet-etching. This model is based on an assumption that a high concentration of oxygen Frenkel defects is formed during deposition and they remain as a result of insufficient structural relaxation near the surface. Notably, the formation of Frenkel pairs is experimentally recognized in amorphous solids like a-SiO_2 because local chemical ordering is preserved in amorphous structure [20]. The simulated transfer characteristics are shown as solid lines in Fig. 1a, and the DOSs used in the simulations are presented in Fig. 1b. The density of surface tail states ($N_{tail,A}$) of CB was increased to reflect the enhanced potential barrier near the CB edge caused by Frenkel-defect-induced structural disorder [6]. In addition, the densities of Gaussian-distributed acceptors and donors are simultaneously increased, and their energy levels are deepened. Note that these defects are located below the observed E_F at the doping carrier concentration of 1×10^{17} cm^{-3}, estimated by Hall effect measurement, and therefore their contribution to carrier transport is negligibly small. For the commercially used In:Ga:Zn= 1:1:1 composition with a low carrier concentration, the E_F may be located within the defect state, potentially causing a threshold voltage (V_{th}) shift and a large subthreshold swing (*SS*). Moreover, TFTs fabricated under high P_{O2} conditions exhibit higher *SS* values compared to those fabricated under low P_{O2} conditions (0.54 and 0.37 V/dec, respectively, for t_{ch} = 5 nm). Based on these results, the variations in the DOS near the E_F under different P_{O2} conditions are represented in the TCAD model by adjusting the acceptor-like trap concentration. The origin of these traps is assumed to correspond to the concentration of CB tail states induced by structural disorder, specifically Frenkel defects. It has been reported that high P_{O2} induces negative ion resputtering during sputtering [8]. We propose that this resputtering could enhance surface damage, thereby increasing the concentration of Frenkel defects and resulting in the formation of a structurally disordered, defective surface layer. Figs. 1c and 1d present the characteristics of IGZO TFTs deposited under high P_{O2} (O-rich) conditions. The surface defect density was increased in the simulation (Fig. 1d), reproducing a thickness-dependent mobility degradation similar to that under oxygen-poor conditions, as well as a characteristic V_{th} shift (Fig. 1a). These results strongly suggest that a high density of CB tail states localized near the back-channel surface predominantly governs the μ_{FE} degradation in the thinner film.

To examine this idea, we examined the electronic structures of the near-surface and bulk regions of a-IGZO thin films by using HAXPES combined with TR [17]. Fig. 2a shows the surface- and bulk-sensitive valence band (VB) spectra of a 100-nm-thick a-IGZO film measured with the TR and non-TR conditions, respectively. The surface-sensitive spectrum exhibits an enhanced density of donor states. This observation can be attributed to an increased fraction of Frenkel defects (structural disorder). Consequently, in thinner films (Fig. 2c),

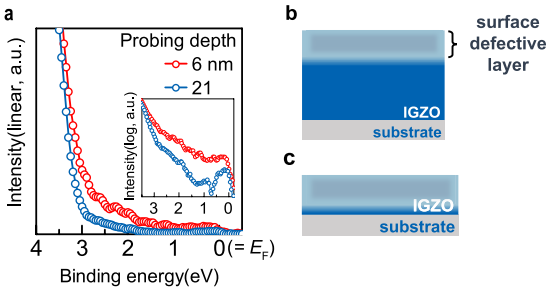

Fig. 2. (a) Depth-dependent VB HAXPES spectra. The surface- and bulk- sensitive spectra were obtained using TR- and non-TR-HAXPES modes, respectively. (b, c) Schematics of the surface defective region and intrinsic bulk region for (b) thick and (c) thin a-IGZO films.

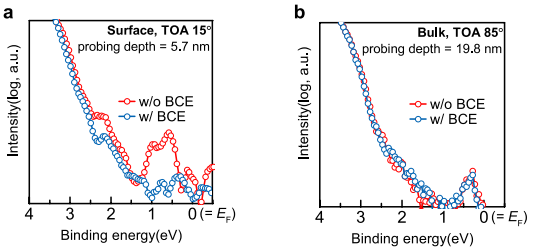

Fig. 3. VB HAXPES spectra obtained at TOAs of (a) 15° (surface-sensitive) and (b) 85° (bulk- sensitive) for a-IGZO thin films before and after BCE.

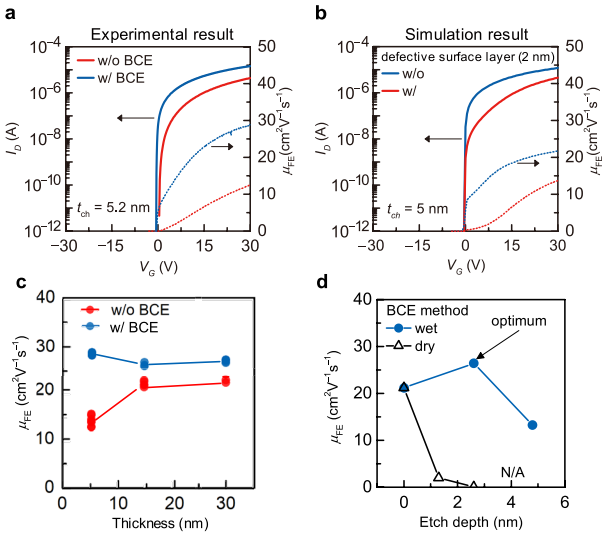

Fig. 4. Improved TFT performance by BCE. (a) Measured transfer characteristics and μ_{FE} of a-IGZO TFTs (t_{ch} = 5.2 nm) with and without BCE. The BCE device was wet-etched (~2.4 nm) from 7.6 nm film. (b) Simulated results for 5 nm TFTs. (c) Measured t_{ch} dependence of μ_{FE} with and without BCE. (d) Measured μ_{FE} variation with etching depth for wet and dry etching.

the volume fraction of this defective surface layer increases relative to the thicker films (Fig. 2b), and thus carrier transport is dominated by the surface defective layer.

In our model, the origin of the CB tail states in a-IGZO is incorporated as structural disorder perturbed by the Frenkel defect. Structural disorder in amorphous oxides induces local electrostatic potential fluctuations, leading to Anderson localization and the broadening of unoccupied tail states below the CBM. This phenomenon is particularly prominent in the surface layer, when Frenkel defects are formed during deposition and remain structurally unrelaxed. Since these high-density Frenkel defects or strained M–O–M bonds should be chemically unstable and sensitive to etching in amorphous oxides, we employed a TMAH-based wet solution to selectively remove the defective surface layer [21], [22]. The normalized VB spectra before and after the back-channel-etch (BCE) are shown in Figs. 3a and 3b. Notably, a clear reduction in defect states near the E_F was observed, while the bulk remains unchanged. This observation can be explained by the reduction in the donor states density; in this case, the decrease in fraction of Frenkel defects leads to a suppression in disorder-induced tail states. Here, the E_F is determined to be 0.05 eV below E_{CBM}, estimated by optical band gap (E_g) (2.85 eV) $-E_{VBM}$ (2.8 eV), which were obtained from E_g measurements and HAXPES, respectively. Note that thermal desorption spectroscopy (TDS) measurements confirmed that H_2 and CO_2 were not detected, thereby excluding hydrogen- and carbon-related impurity effects.

The 5.2 nm t_{ch} TFTs showed a significant improvement in μ_{FE} after the BCE (Fig. 4a), increasing from 13.7 to 28.5 cm^2/V·s due to suppression of surface traps. A similar enhancement was also observed for the 15 and 30 nm TFTs (Fig. 4c). This improvement can be attributed to the removal of the defective surface layer, which enhances front-channel transport by mitigating defect states, even in thicker TFTs.

To examine the origin of the improvement, TCAD simulations were performed (Fig. 4b). By removing the surface layer with a high density of tail states from the bilayer model (upper panel of Fig. 1b), the simulations reproduce the restored transfer characteristics. This result indicates that the removal of the defective surface layer is the dominant factor in restoring the μ_{FE} by reducing the concentration of tail states at the back channel. It is observed that μ_{FE} increases as the etching depth approaches ~2.5 nm but subsequently exhibits deterioration (Fig. 4d). This degradation may be attributed to the stoichiometric imbalance or morphological effect induced by prolonged selective etching. In contrast, the dry-etched TFTs exhibited severe degradation, which is attributed to the formation of plasma-induced damage by Ar^+ ion sputtering at the back-channel [23].

IV. Conclusion

The defective surface layer was identified as the major origin of μ_{FE} degradation in ultra-thin a-IGZO TFTs. Experimental and TCAD analyses revealed that the deterioration correlates with a high density of tail states below the CBM. This finding indicates perturbations of the CB edge, where a high density of defects induces potential fluctuations, broadening the tail states. Such structural disorder originates from insufficient relaxation of the as-deposited thin film. Based on the proposed model, the deterioration in the ultra-thin regime can be overcome by removing the defective surface region via a wet-etching process. Consequently, we achieved the 5 nm t_{ch} a-IGZO TFT with high μ_{FE} of 28.5 cm^2/V·s, comparable to that of thick channel devices.

Acknowledgment

The HAXPES measurements were performed with the approval of JASRI/SPring-8 (Proposal Nos. 2025A1748, 2025A1524, 2025B1622, and 2025B1875).

REFERENCES

[1] K. Nomura, H. Ohta, A. Takagi, T. Kamiya, M. Hirano, and H. Hosono, "Room-temperature fabrication of transparent flexible thin-film transistors using amorphous oxide semiconductors," *Nature*, vol. 432, no. 7016, pp. 488–492, Nov. 2004, doi: 10.1038/nature03090.

[2] Y. Kuo, H. Hosono, M. S. Shur, and J. Jang, *Oxide Thin Film Transistors*. Hoboken, NJ, USA: Wiley, Nov. 2024.

[3] S. Samanta, K. Han, C. Sun, C. Wang, A. Kumar, A. V.-Y. Thean, and X. Gong, "Amorphous InGaZnO thin-film transistors with sub-10-nm channel thickness and ultrascaled channel length," *IEEE Trans. Electron Devices*, vol. 68, no. 3, pp. 1050–1056, Mar. 2021, doi: 10.1109/TED.2020.3048920.

[4] J. Y. Kim, H. Kim, D. Kim, and H. W. Jang, "Advancements of amorphous IGZO-based transistors: Materials, processing, and devices," *ACS Appl. Electron. Mater.*, vol. 7, no. 11, pp. 4703–4728, Jun. 2025, doi: 10.1021/acsaelm.5c00605.

[5] A. Belmonte, H. Oh, N. Rassoul, G. L. Donadio, J. Mitard, H. Dekkers, R. Delhougne, S. Subhechha, A. Chasin, M. J. van Setten, L. Kljucar, M. Mao, H. Puliyalil, M. Pak, L. Teugels, D. Tsvetanova, K. Banerjee, L. Souriau, Z. Tokei, L. Goux, and G. S. Kar, "Capacitor-less, long-retention (>400s) DRAM cell paving the way towards low-power and high-density monolithic 3D DRAM," in *IEDM Tech. Dig.*, Dec. 2020, pp. 28.2.1–28.2.4, doi: 10.1109/IEDM13553.2020.9371900.

[6] H. Cho, M. Tsuji, S. Ueda, J. Kim, and H. Hosono, "Oxygen defects and instability in very thin a-IGZO TFTs," *Adv. Electron. Mater.*, vol. 11, no. 15, p. e00349, Sep. 2025, doi: 10.1002/aelm.202500349.

[7] L. Shao, K. Nomura, T. Kamiya, and H. Hosono, "Operation characteristics of thin-film transistors using very thin amorphous In–Ga–Zn–O channels," *Electrochemical Solid-State Lett.*, vol. 14, no. 5, p. H197, May 2011, doi: 10.1149/1.3555070.

[8] T.-H. Chiang, B.-S. Yeh, and J. F. Wager, "Amorphous IGZO thin-film transistors with ultrathin channel layers," *IEEE Trans. Electron Devices*, vol. 62, no. 11, pp. 3692–3696, Nov. 2015, doi: 10.1109/TED.2015.2478700.

[9] M. Kimura, T. Nakanishi, K. Nomura, T. Kamiya, and H. Hosono, "Trap densities in amorphous-$InGaZnO_4$ thin-film transistors," *Appl. Phys. Lett.*, vol. 92, no. 13, Mar. 2008, Art. no. 133512, doi: 10.1063/1.2904704.

[10] M. J. Kim, H. J. Park, S. Yoo, M. H. Cho, and J. K. Jeong, "Effect of channel thickness on performance of ultra-thin body IGZO field-effect transistors," *IEEE Trans. Electron Devices*, vol. 69, no. 5, pp. 2409–2416, May 2022, doi: 10.1109/TED.2022.3156961.

[11] K. Abe, K. Nomura, T. Kamiya, and H. Hosono, "Optical evidence for quantization in transparent amorphous oxide semiconductor superlattice," *Phys. Rev. B, Condens. Matter*, vol. 86, no. 8, Aug. 2012, Art. no. 081202, doi: 10.1103/physrevb.86.081202.

[12] T. Kim, H. Jang, B. Park, S. Shin, M. A. Alam, P. D. Ye, and C. Jeong, "Engineering amorphous IGZO thin-film transistors: The role of composition and channel thickness in mobility-threshold voltage optimization," *ACS Omega*, vol. 10, no. 50, pp. 62182–62188, Dec. 2025, doi: 10.1021/acsomega.5c09705.

[13] S. Kim, Y. Lee, S. Shin, H. Kim, H. Shin, H. Hosono, C. Jeong, and J. Kim, "Mobility overestimation in thin-film transistors: Effects of device geometry and fringe currents," *ACS Nano*, vol. 19, no. 41, pp. 36614–36625, Oct. 2025, doi: 10.1021/acsnano.5c11904.

[14] T. Takahashi and Y. Uraoka, "Intrinsic field-effect mobility in thin-film transistor with polycrystalline In_2O_3 channel based on transfer length method," *Appl. Phys. Exp.*, vol. 18, no. 1, Jan. 2025, Art. no. 014001, doi: 10.35848/1882-0786/ada19e.

[15] M. M. Billah, M. D. H. Chowdhury, M. Mativenga, J. G. Um, R. K. Mruthyunjaya, G. N. Heiler, T. J. Tredwell, and J. Jang, "Analysis of improved performance under negative bias illumination stress of dual gate driving a-IGZO TFT by TCAD simulation," *IEEE Electron Device Lett.*, vol. 37, no. 6, pp. 735–738, Jun. 2016, doi: 10.1109/LED.2016.2557358.

[16] K. Abe, A. Sato, K. Takahashi, H. Kumomi, T. Kamiya, and H. Hosono, "Mobility- and temperature-dependent device model for amorphous In–Ga–Zn–O thin-film transistors," *Thin Solid Films*, vol. 559, pp. 40–43, May 2014, doi: 10.1016/j.tsf.2013.11.066.

[17] S. Ueda, "Depth-resolved electronic structure measurements by hard X-ray photoemission combined with X-ray total reflection: Direct probing of surface band bending of polar GaN," *Appl. Phys. Exp.*, vol. 11, no. 10, Oct. 2018, Art. no. 105701, doi: 10.7567/apex.11.105701.

[18] S. Ueda, Y. Fujita, and Y. Sakuraba, "Near-interface electronic and magnetic states of insulator/Co_2MnSi heterostructures probed by hard X-ray photoemission combined with X-ray total reflection," *Phys. Rev. B, Condens. Matter*, vol. 109, no. 8, Feb. 2024, Art. no. 085109, doi: 10.1103/physrevb.109.085109.

[19] A. Yasui, Y. Takagi, T. Osaka, Y. Senba, H. Yamazaki, T. Koyama, H. Yumoto, H. Ohashi, K. Motomura, K. Nakajima, M. Sugahara, N. Kawamura, K. Tamasaku, Y. Tamenori, and M. Yabashi, "BL09XU: An advanced hard X-ray photoelectron spectroscopy beamline of SPring-8," *J. Synchrotron Radiat.*, vol. 30, no. 5, pp. 1013–1022, Sep. 2023, doi: 10.1107/s160057752300629x.

[20] H. Hosono, Y. Ikuta, T. Kinoshita, K. Kajihara, and M. Hirano, "Physical disorder and optical properties in the vacuum ultraviolet region of amorphous SiO_2," *Phys. Rev. Lett.*, vol. 87, no. 17, Oct. 2001, Art. no. 175501, doi: 10.1103/physrevlett.87.175501.

[21] H. Hosono, "Fourier transform infrared attenuated total reflection spectra of ion-implanted silica glasses," *J. Appl. Phys.*, vol. 69, no. 12, pp. 8079–8082, Jun. 1991, doi: 10.1063/1.348925.

[22] Y. Shi, Y.-S. Shiah, K. Sim, M. Sasase, J. Kim, and H. Hosono, "High-performance a-ITZO TFTs with high bias stability enabled by self-aligned passivation using a-GaO_x," *Appl. Phys. Lett.*, vol. 121, no. 21, Nov. 2022, Art. no. 212101, doi: 10.1063/5.0123253.

[23] G. W. Mattson, K. T. Vogt, J. F. Wager, and M. W. Graham, "Illuminating trap density trends in amorphous oxide semiconductors with ultrabroadband photoconduction," *Adv. Funct. Mater.*, vol. 33, no. 25, Jun. 2023, Art. no. 2300742, doi: 10.1002/adfm.202300742.